Contents list available at CBIORE journal website

International Journal of Renewable Energy Development

Journal homepage: https://ijred.cbiore.id

Research Article

Comparative study of Reynolds number and Flowrate effects on the thermal–hydraulic performance of corrugated channels with winglets using TiO_2 nanofluids

Shadan Kareem Ameen [a*] and Adnan Muhammed Hussein[a,b]

[a]*Department of Mechanical Engineering, Kirkuk Technical Engineering College, Northern Technical University, Iraq.*

[b]*Renewable Energy Research Center Kirkuk, Northern Technical University, Kirkuk, Iraq.*

Abstract. This study aims to provide a deeper and more realistic understanding by conducting a systematic comparison between the two approaches (Reynolds number and volumetric flowrate). The analysis emphasizes the impact of internal channel design, using inclined winglets and surface corrugation. An experimental investigation was carried out to prepare and characterize a TiO_2/H_2O nanofluid at 1% volume concentration, including accurate measurements of its thermophysical properties and stability validation. A numerical model was also developed using ANSYS Fluent to simulate the hydrothermal behavior of two channel configurations (straight and corrugated), in which the effects of both Reynolds number and flowrate were evaluated across key parameters such as heat transfer coefficient, pressure drop, performance evaluation criterion, and wall temperature distribution. By observing the flow patterns inside the corrugated channel, three distinct flow behaviors were identified: axial flow along the channel, transverse flow induced by winglets, and swirling flow within the corrugated grooves. This combination of flow modes enhanced fluid mixing and significantly improved heat transfer performance. The results show that TiO_2 nanofluid significantly enhances the thermal–hydraulic performance, with the relative friction factor (Γ) increasing from 6.9 to 7.6 and the thermal enhancement ratio (En) reaching 2.8 (PEC ≈ 1.5) when evaluated using Reynolds number, while volumetric flow rate assessment (7–9 L/min) yielded higher Γ (3.9–4.2) and En/PEC (2.5/1.6). The effects of the internal enhancement techniques were found to be more pronounced when using flowrate as the reference indicator. This work represents a valuable scientific contribution by integrating three advanced enhancement strategies (surface corrugation, inclined winglets, and nanofluid), and it highlights the need to reconsider traditional thermal system design methods based solely on Reynolds number.

Keywords: Corrugation surface; Winglets; Heat transfer; Relative friction factor; Thermal enhancement ratio; Hydrothermal performance.

Received: 14th Oct 2025; Revised: 16th January 2026; Accepted: 20th January 2026; Available online: 27th January 2026

1. Introduction

The challenge of enhancing the hydrothermal performance of heat exchangers is a significant focus for researchers in thermal engineering, particularly in heat transfer (HT) (Sedeeq, Ameen, and Bolatturk 2018). Several approaches have been offered to agminate HT efficiency with the penalty of increasing in pressure losses(ΔP) including active, passive, and compound flow control approach (Hussein and Yagoob 2021; Salami, Khoshvaght-Aliabadi, and Feizabadi 2019). The enhancement is associated with the decrease mass, minimize size, lower costs, and increase the HT rate, which is necessary for various technical applications. One of the most crucial methods to enhance heat transfer rate is to develop the path of the working fluid using corrugations inside channel surface. This technique enables secondary flow vortices, which acuminated fluid mixing and achieves the desired level of improvement (Hussein et al. 2013).

Various researches have been conducted in various pattern on HT using conventional fluid and nanofluid in different forms of corrugated channel (CC). A study (Hosseinpour, Kazemeini, and Rashidi 2020) conducted research to examine how the thermal and hydraulic performance of a Finned Micro channel Heat Sink is affected by its shape and operating circumstances. The study evaluated four different forms of microfine: (conical, pyramidal, cylindrical, and cubical). The findings indicated that Reynolds number (Re) was the most influential factor for the conical and pyramidal. The most significant impacts on cylindrical shape were seen in the change of diameter of the fins.

Studies conducted by Karabulut (Karabulut 2020) and Alnak (Alnak 2020), focused on numerical investigating the impact of varying placement angles of baffles on HT and Δp. The Re range under investigation was 1000-6000, while the baffle placing angles being considered are 30°, 45°, 60°, and 90°. The only difference between the two publications is in the configuration of the baffles. Karabulut used triangular baffles, while Alnak employed rectangular baffles. According to Nusselt number (Nu) viewpoint, when comparing the two studies above, it is shown that triangle baffles with a 60° angle are more effective than those with a 90° angle. In rectangular baffles, the opposite phenomenon occurs. When comparing the findings based on Δp, it is seen that both triangular and rectangular baffles exhibit the maximum value at a 90° angle.

* Corresponding author
Email: ameenshadan@ntu.edu.iq (S. K.Ameen)

https://doi.org/10.61435/ijred.2026.61883
ISSN: 2252-4940/© 2026.The Author(s). Published by CBIORE

In an another study (Li et al. 2022), the researchers performed that presence of baffles in the flow channel introduces additional complexity due to the differences in apex angle and baffle location. The results showed that the flow channels with a 60° or 90° apex angle have similar values of friction factor (ʃ), which are higher than those with a 120°. A similar pattern was seen with Nu.

An analysis was conducted employing pulsing flow in CC (Akcay 2022). They measured the impact of pulsing flow on the hydrothermal performance of CC equipped with V-type winglets. The study examined three distinct channel flows, each with a different configuration (non-winglet, solid winglet, and perforated winglet). The results indicated that the pulsation parameters had a substantial role in enhancing HT, particularly at high Re. It was noted that the presence of perforated winglets decreased the (ʃ) compared to the solid winglets.

Another research study is being conducted on using winglets in corrugated walls (Their, Azeez, and Mohsin 2023). This research examines how HT and Δp features in rectangular channels which improved by using transverse corrugations and longitudinal winglet vortex generators. The numerical simulations included Re ranging from 5000 to 20000. The results showed that corrugated walls with winglets have a Nu of 67.7% greater than smooth and 61.8% higher than CC without winglets.

Corrugated wall Combined with Backward-Facing Step (BFS) is also another demanded corrugation. The studies (Hilo *et al.* 2020; Koca 2022) focused on the numerical investigation of the turbulent water flow by combining BFS with different corrugated walls such as (zigzag, triangular, and trapezoidal). The researchers found a substantial enhancement of HT while causing a minor rise in (ʃ). The trapezoidal corrugation with a height of 4 mm showed the most effective enhancement in HT.

Rahman, Islam, and Khan (2023) performed a numerical analysis to study HT and Δp properties of small rectangular channels with rib-roughened surfaces and heat supply. Numerical data sets are produced using three different corrugation pitch to height ratios (p/e). These data sets include both one and two-sided ribbed walls, as well as one and two-sided heat supply. In conclusion, the channel with (p/e) ratio of 8 had superior HT capabilities and a more noticeable Δp.

The study by Ramgadia and Saha (2016) investigated asymmetric wavy-walled shapes for fully developed flow and HT numerically. The hydrothermal performance of wavy-walled configurations is evaluated for three phase shift angles between heated walls. The study discovered that the asymmetric geometry with 0o phase shift exhibits the most significant flow imbalance close to the centerline.

A Computational Fluid Dynamic (CFD) model is used to explore several NF including (GNP-SDBS, Al_2O_3, SiO_2) and tube geometries (rectangular, triangular, trapezoidal, curved ribs) (Kaood and Hassan 2020). The largest overall performance gain, around 37%, was seen in the case of GNP-SDBS/water flow in a curved ribbed tube at Re of 10,000 when compared to distilled water (DW) flow in a smooth tube.

The study of Javadpour *et al.* (2020) seeks to create and evaluate a numerical model to predict the Nu and (ʃ) based on ribbed length, height, distance between ribs, and volumetric concentration (Φ). of Al_2O_3/H_2O nanofluid in laminar flow. Numerical analysis of rib forms (triangular, rectangular, and trapezoidal) were performed using the Taguchi technique. The calculation confirmed the effectiveness of the projected parameters for optimal response function design, with a 40% Nu and 16% (ʃ).

The research of Bhowmick, Randive, and Pati (2021) conducted numerical analysis to investigate the hydrothermal properties of forced convection in CC which has several profiles, including (triangular, sinusoidal, and trapezoidal) shapes. Additionally, a single layer of porous foam made of aluminum is integrated into the channels core. The results were obtained by varying the Re and (Φ). of nanofluid. The results demonstrate that the trapezoidal channel exhibits superior enhancement in HT and the performance evaluation criterion (PEC) if compared with straight channel (SC).

A numerical investigation was conducted to study the forced convection flow of water/Carboxy-Methyl Cellulose NF in three wavy and straight channels (Shahsavar *et al.* 2021). The findings indicated that the impact of Re on Nu is much more significant than that of (Φ). In addition, the sinusoidal channel has the most considerable Nu value compared to the other channels. Baffles and corrugations are effective passive technic by disturbing hydrodynamic and thermal boundary layers. (Raheem K Ajeel, Zulkifli *et al.* 2021; Raheem K Ajeel, Sopian, and Zulkifli 2021; Raheem Kadhim Ajeel, Sopian, and Zulkifli 2021) focus on numerical investigating the flow structure and HT properties of a novel channel design called the (curved corrugated channel). The studies specifically examine the use of ZnO/H_2O and CuO-MgO/ H_2O as NF with the inclusion of (L-shaped or E-shaped) baffles. The effect of corrugation with baffles arrangement are assessed at various Re and (Φ). The findings demonstrate that corrugations and baffles may lead to vortex flow and increased turbulence, resulting in enhanced (HT). The optimum (PEC) of 1.99 is achieved when the baffles are positioned at an angle of at least 30°.

The research (Naderifar *et al.* 2022) numerically examined the flow structure and HT improvement of a non-Newtonian NF in a corrugated channel with fins. The presence of fins causes a significant alteration in the flow and improvement in HT ratio. Moreover, the findings indicated that using two corrugations in the channel yields a superior HT rate compared to other corrugations. A numerical study of a microchannel for Al_2O_3/H_2O nanofluid in laminar flow was investigated (Shamsi et al. 2017). Nanoparticles with various diameter size and (Φ) were used in the study. The findings showed that increasing (Φ) and using nanoparticles with smaller diameters result in better HT enhancement. The triangular rib with a 30° angle of attack has the highest Nu and the lowest Δp in the microchannel among all studied configurations.

The research (Abed et al. 2015) investigated a numerical study of turbulent flow and HT in trapezoidal channels using of nanoparticles of Al_2O_3, CuO, SiO_2, and ZnO with DW as working fluid. The study presented that SiO_2/H_2O had the highest Nu among other NF. The most PEC settings were seen at CuO/H_2O with 2.5 mm of corrugation height, and 6 mm of corrugation pitch.

A numerical simulation of turbulent flow and HT of Al2O3/H2O nanofluid within a rectangular channel was conducted (Parsaiemehr et al. 2018). The examining has been conducted on changes in the attack angle of ribs within the range of 0 to 180°. The results indicate that variations in the attack angle of ribs, caused by changes in the flow pattern and the formation of vortices within the channel, which affect fluid mixing significantly.

A research conducted a numerical analysis to examine the impact of pulsing NF stream on the flow and HT in a semicircular corrugated channel with vertical baffles (Akcay 2023). The top surface of the channel was treated as adiabatic condition and had vertical baffles. The bottom surface of the semicircular CC was maintained at constant temperature of 350 K. The working fluid used was CuO particles dispersed in water. The findings showed a substantial enhancement in HT when the pulsing parameters were applied at a high input velocity.

Thermal enhancement ratio (En) for the pulsing flow also increased by about 2.6 times compared to the constant flow of the base fluid in the channel without baffles.

Another studies by same researcher (AKÇAY 2021, 2023) investigated thermo-hydraulic performance of an Al_2O_3/H_2O nanofluid in a zigzag channel with baffles numerically. The channels bottom and top zigzag surfaces were maintained at a constant temperature, allowing for calculating Nu and (ʃ) along the channel. The findings indicated that higher (Φ) and Re led to enhanced in HT, although with a slight increase in (ʃ). The optimal PEC was achieved at a Re of 1400 and (Φ) of 0.03, resulting in a value of 1.15.

An investigation was conducted on HT properties of Al_2O_3/H_2O nanofluid inside CC, including a flat blade (Hekmat and Saharkhiz 2022). A total of 380 simulations were conducted to investigate the combined impacts of the blade's scenario (stationary or oscillating) and the channel walls shape (straight or corrugated) on thermal-hydraulic performance The analysis revealed that by turning on the oscillating blade when the Re are high and turning it off when the Re are low, leads to a substantial enhancement in PEC.

A numerical study investigates hydrothermal performance for CC by considering the combined effect of inclined ribs and NF of CuO-MgO nanoparticles dispersed in water (Hamad and Ajeel 2022). Researchers have shown that ribs with a 90° attack angle are more flow desirable than ribs with a smaller attack angle for achieving the best hydrothermal performance in a channel. Additionally, the height of the ribs is the most significant factor affecting (ʃ) of fluid flow in the channel.

An analysis focuses on the flow of a Cu/H_2O and Ag/H_2O nanofluid through a channel that has been improved with 45°V-shaped baffles (Bahiraei, Mazaheri, and Moayedi 2020). Initially, a comparison is conducted between 45° and 60° attack angles, revealing the advantage of the 60° angle due to its reduced entropy generation. In addition, the inserted V-shaped baffles significantly help to reduce irreversibility by producing various recirculation flows and strong swirl flows. The researchers observed that the simultaneous use of increased baffle height and smaller baffle pitch results in less exergy destruction and improved second law efficiency.

A novel research explores the numerical study proposes a new approach to improve the performance of a Thermo-electric Generator module positioned between channels that transport hot and cold fluid streams (Selimefendigil and Öztop 2020). The technique involves using both types of surface corrugation and a hybrid NF. The study investigates the effects of Re, groove number, corrugation height, and type (rectangular and circular), as well as (Φ) of the NF, on power generation. The results indicated that the power increases by about 10.95% when the Re is 250, while it increases by 7.50% when the (Re) is 1000, with (Φ) of 0.02. The corrugation height has a more significant influence on the produced power than the number of waves in the groove.

Upon careful analysis of previous studies, it becomes evident that most research on improving hydrothermal performance in channels has primarily relied on the Re as the main criterion for evaluating flow and HT characteristics. Although Re is clearly important for describing the flow regime, relying on it alone may not reflect the actual performance of thermal systems operating under fixed or limited flow rates, as is often the case in industrial applications. On the other hand, some studies have shown that integrating surface corrugation with inclined winglets, especially when using nanofluids, can significantly enhance heat transfer with minimal pressure losses, thus improving overall heat exchanger performance. Based on these insights, the proposed study aims to conduct a systematic comparison between the effects of Reynolds number (Re) and volumetric flow rate (FR) on hydrothermal performance of channels equipped with internal enhancement features (corrugations and winglets), using TiO_2/H_2O nanofluid that was experimentally prepared and tested at 1% volume concentration. The goal of this comparison is to evaluate how each parameter (Re or FR) influences key thermal characteristics such as the temperature difference between inlet and outlet (ΔT_{fluid}), channel surface temperature ($T_{surface}$), and convective heat transfer coefficient (h), in addition to dimensionless performance indicators including thermal enhancement ratio (En), relative friction factor (Γ), and performance evaluation criterion (PEC). This comparison will support researchers and engineers in selecting the most suitable evaluation method when designing thermal systems, helping to achieve both accurate predictions and higher operational efficiency. In this context, the study poses a key question: which approach (Re or FR) offers a more realistic representation of performance in enhanced thermal channels?

2. Preparation and experimental testing of TiO_2 nanofluid

Distilled water was produced using a (Nukieon-SS 200) distillation unit and used as the base fluid for nanofluid preparation. TiO_2 (anatase) nanoparticles were dispersed in DW at a volume concentration of 1% using a magnetic stirrer for 60 minutes, followed by ultrasonic treatment to promote uniform dispersion. The preparation procedure was designed to obtain a homogeneous NF suitable for short-duration experimental investigations. During the experimental campaign, no visible sedimentation or phase separation was observed under the applied operating conditions.

The thermophysical properties of DW and NF were determined experimentally and subsequently employed directly in the numerical simulations to ensure consistency between experimental measurements and CFD modeling. Density was measured using a digital densitometer (Mettler Toledo-30 px), dynamic viscosity using Fungilab and Biobase viscometers, and thermal conductivity was measured by the transient hot-wire method using a thermal property analyzer (KD2 Pro System, Decagon Devices). The specific heat capacity was evaluated analytically using the Pak and Cho correlation (Pak and Cho, 1998). All thermophysical properties were measured immediately after nanofluid preparation to ensure that the reported values correspond to the freshly dispersed state used in the experiments.

Table 1 presents the values of density, dynamic viscosity, thermal conductivity, and heat capacity for TiO_2 nanoparticles, distilled water, and NF at 1% volume concentration both theoretically and experimentally. The data clearly show that

Table 1
Thermophysical properties.

	Density, ρ (kg/m^3)	Heat capacity, Cp (J/kg K)	Dynamic viscosity, μ (mPa.s)	Thermal conductivity, λ (W/m K)
TiO_2 (solid)	3900	686.2	---	7.95
DW (Exp.)	996	4182	1.1	0.601
NF (Exp.)	1019.3	----	1.6	0.64
NF (Num.)	1025.04	4048.994	1.127989	0.615954

introducing TiO_2 nanoparticles into DW at this concentration causes noticeable changes in the thermophysical properties of the fluid. A comparison examination of the results with those of (Zhong, Zhong, and Wen 2020). indicated percentage variations of around 1.5%, 8.3%, and 3.4% in (ρ), (μ), and (λ), respectively. Although these differences, the error margins remained within acceptable bounds as documented in the literatures (Zhong et al. 2020), (Turgut et al. 2009), and. (Murshed, Leong, and Yang 2005). Consequently, the current findings appear valid and reliable, especially because they are evaluated within a system of standard experiments published in NF research. Therefore, the experimental values were used at conducting the simulation of the channel.

3. Channel geometry and simulation setup

As shown in Figure. 1 of the imagined channel geometry, the CC consists of a rectangular cross-section channel including dimensions of 40mm width, 500mm length (L), 12.5mm channel height. It has rectangular corrugated grooves on the upper surface and winglet within the lower surface. The upper corrugated wall forms as a wavy unit. The profile of each wavy unit is given by 10mm corrugation pitch and 2.5mm corrugation height. The lower surface has winglets with a height of 2.5mm, width of 2mm, and length of 7mm in the form of a V-shape with a perforation in the middle at an angle of 60°.

The flow and HT in CC are numerically simulated using the Ansys Fluent 19.3-CFD program. 3-D models. Based on the output of the experimental measurement, the thermophysical characteristics of the working fluid are held constant. Furthermore, the assumption is made that there is no HT by thermal radiation, and the influence of gravity is disregarded. The simulations are conducted exclusively under situations of constant input velocity according to Re within the range of 4433 to 5700 and FR within the range of 7 to 9 Lpm. From the previous presumptions, the governing equations in tensor form can be expressed as follows (Bazdidi-Tehrani, Karami, and Jahromi 2011; Benim, Chattopadhyay, and Nahavandi 2011):

Continuity equation;

$$\frac{\partial}{\partial x_i}\left(\rho \bar{u}_i\right) = 0 \quad (1)$$

Momentum equation;

$$\frac{\partial}{\partial t}(\rho \bar{u}_i) + \frac{\partial}{\partial x_j}(\bar{u}_i \bar{u}_j) = -\frac{\partial \bar{p}}{\partial x_i} + \frac{\partial}{\partial x_j}\left[(\mu + \mu_t)\left(\frac{\partial \bar{u}_i}{\partial x_j} + \frac{\partial \bar{u}_j}{\partial x_i}\right)\right] - \rho \overline{\acute{u}_i \acute{u}_j} \quad (2)$$

Where;

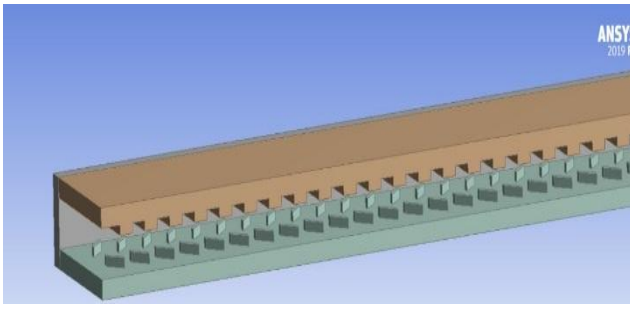

Fig 1. The schematic geometry of the channel.

$$-\rho \overline{\acute{u}_i \acute{u}_j} = (\mu_t)\left(\frac{\partial u_t}{\partial x_i} + \frac{\partial u_i}{\partial x_i}\right) \quad (3)$$

And (μ_t) is the turbulent viscosity, computed by combining k and ε by which is described as:

$$\mu_t = \rho C_\mu \frac{k^2}{\varepsilon} \quad (4)$$

Energy equation;

$$\frac{\partial}{\partial t}\bar{T} + \frac{\partial}{\partial x_j}(\rho \bar{u}_i \bar{T}) = \frac{\partial}{\partial x_j}\left[(\tau + \tau_t)\left(\frac{\partial \bar{T}}{\partial x_j}\right)\right] \quad (5)$$

4. Boundary conditions

The inlet velocity profile of the flow within the solution domain is assumed to be uniform, with a constant temperature of 27 °C. No-slip condition applies to all walls within the solution domain. Upper and lower walls of the test model experience a constant heat flux (HF) of 10 kW/m^2, whereas the side walls are adiabatic. The outlet pressure scale is established at zero. Turbulence intensity (It) can be calculated by Eq. 6, which derived from the empirical correlation of pipe flow (Cengel and Chajar 2015).

$$I_t = 0.16\, Re^{-1/8} \quad (6)$$

5. Mesh independent and verification of (Nu) and (*f*) results.

Figure 2 demonstrates using an unstructured triangular grid to discretize the flow domain within the CC. The figure illustrates that the mesh has grown with multiple uniform layers adjacent to the solid-liquid interfaces to satisfy the boundary layer thickness requirements ($y^+ < 1$).

A mesh independence test ensures that the numerical results remain consistent regardless of the number of elements in the grid. Six different meshes are analyzed, with an increasing range of elements from 18,360 to 3,870,000 for this evaluation. Figure 3 illustrates the grid sensitivity analysis in terms of both the Nu, represented by red bars and (*f*), represented by blue curve. The results were assessed at Re and HF of 5000 and 10

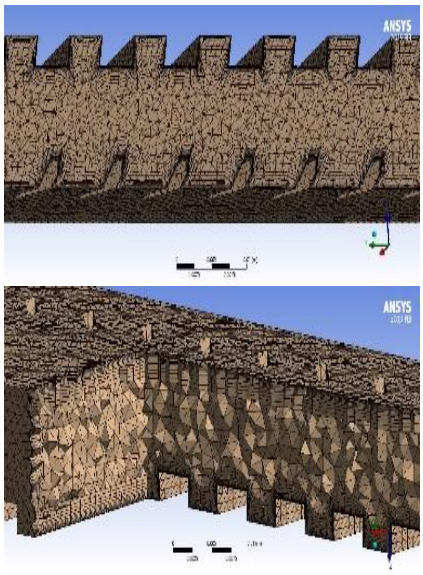

Fig 2. Mesh structure.

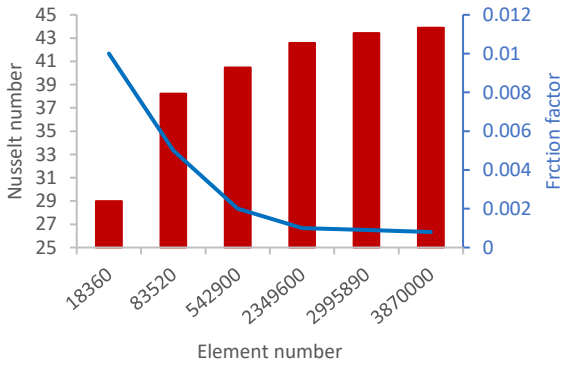

Fig 3. Nu and (ʃ) values for variable element number.

kW/m², respectively. It is observed that both parameters become nearly insensitive to further mesh refinement beyond approximately 230,000 elements, indicating that the selected mesh ensures grid-independent thermal and hydraulic predictions. Hence, the mesh, which includes 2,349,600 elements, was employed for the subsequent simulations in this work.

To validate the reliability of the employed numerical results, forced convection water flow within a corrugated heated channel was investigated. The validation is conducted utilizing Nu and (ʃ) derived from numerical, with values sourced from the Gnielinsky equation and petukhov correlation, as defined in Eq. 7 and Eq. 8 respectively (Cengel and Chajar 2015).

$$Nu = \frac{(f/8)RePr}{1.07+12.7(f/8)^{1/2}(Pr^{2/3}-1)} \quad (7)$$

$$f = (0.79\,ln\,Re - 1.64)^{-2} \quad (8)$$

Figure 4 presents a comparison of the average Nu and Darcy friction factor (*f*) of numerical data with the Gnielinsky and petukhov correlations across various Re. The results demonstrate a clear agreement between the numerical estimation and the correlations as both follow the same overall trends predicted. The slight deviations may be observed to the Gnielinski correlation for heat transfer prediction generally exhibits an average deviation within ±10%, while the Petukhov correlation for friction factor estimation shows an average error of about ±8%, which confirms the consistency between the obtained numerical estimation with the correlations. Therefore,

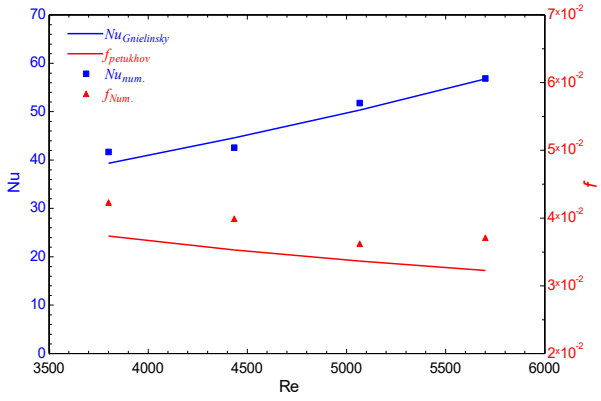

Fig 4. validation of Nu and (ʃ).

the current analyses can be considered reliable and may be confidently adopted in the subsequent stages of this research.

Although a good agreement is observed between the numerical results and the classical correlations, a slight discrepancy between the numerical predictions and experimental data becomes more noticeable at higher Reynolds numbers. This behavior can be attributed to the increased complexity of turbulent flow structures at elevated Reynolds numbers, which may not be fully captured by the employed turbulence model. In addition, experimental factors such as nanoparticle agglomeration, minor variations in thermophysical properties, and measurement uncertainties may further contribute to the observed deviations.

6. Results

In general, both Re and FR are fundamental parameters for evaluating the performance of thermal systems; however, they influence the interpretation of results in different ways. When Re is adopted as the reference parameter, any variation in fluid properties, such as (ρ) or (μ) due to nanofluid addition, or changes in channel geometry, requires a corresponding adjustment in flow velocity to maintain a constant Re. This velocity adjustment directly affects both thermal and hydraulic characteristics, which may obscure the isolated effects of fluid properties or geometric modifications. In contrast, using the FR as the governing parameter provides a more stable experimental condition, as it maintains a constant amount of fluid passing through the system regardless of changes in thermophysical properties or channel configuration. Consequently, FR-based analysis enables a clearer assessment of the individual contributions of nanofluid properties and surface geometry. Moreover, in most practical thermal systems and industrial applications, such as heat exchangers and cooling devices, operating conditions are commonly controlled based on FR rather than Re. Therefore, incorporating FR analysis enhances the practical relevance of the experimental findings, while Re-based approach reflects the combined influence of velocity and fluid properties. The comparative use of both parameters thus provides a more comprehensive understanding of the thermal-hydraulic behavior of the investigated system.

6.1 Flow structure and velocity vectors

Figure 5 illustrates the flow structure inside the corrugated channel with inclined winglets using velocity vector distributions at different views, providing a detailed insight into the flow mechanisms responsible for HT enhancement. As shown in Figure 5(a), the velocity vectors over the lower surface reveal that the inclined winglets strongly deflect the incoming flow, generating intense secondary motions and localized vortices downstream of each winglet. A portion of the core flow is redirected laterally toward the sidewalls due to the pressure gradient induced by the winglets. This lateral deflection significantly enhances near-wall mixing and disrupts the hydrodynamic boundary layer along the lower surface.

The side view presented in Figure 5(b) further confirms this behavior, where the deflected flow impinges on the sidewalls and is redirected upward toward the upper surface. This upward motion promotes strong cross-stream interaction between the lower winglet-induced vortices and the upper corrugated grooves. The interaction between these flow structures leads to a three-dimensional swirling motion, which suppresses stagnant zones and enhances fluid renewal near the heated walls.

In Figure 5(c), the top view inside the corrugated grooves demonstrates that the redirected flow entering the grooves

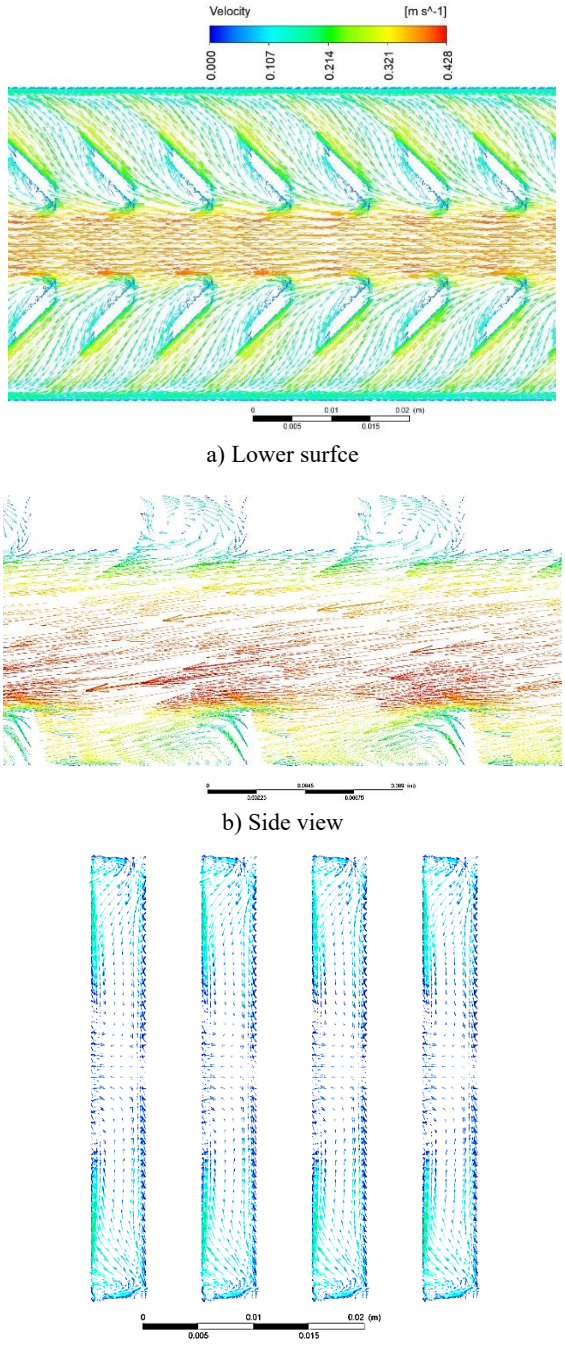

a) Lower surfce

b) Side view

c) Top view for upper grooves

Fig 5. Velocity vectors in the corrugated channel with winglets: (a) lower surface, (b) side view, and (c) top view.

exhibits a rotational and helical motion. This behavior weakens flow separation within the grooves and prevents the formation of low-velocity regions. The flow emerging from opposite sidewalls converges toward the channel centerline, producing a continuous exchange between the core flow and near-wall regions.

Overall, the combined action of the inclined winglets on the lower surface and the corrugated grooves on the upper surface results in sustained boundary-layer disruption, enhanced flow mixing, and improved convective heat transfer performance. This flow mechanism explains the observed enhancement in heat transfer coefficient and thermal-hydraulic performance reported in the subsequent sections.

6.2 Comparison Between (Re) And (FR) according to:

This section compared between Re-based and FR-based analyses. The comparison focused on evaluating thermal and hydraulic performance indicators, including (h), (En), (Γ), (PEC), temperature differential between inlet and outlet (ΔT_{fluid}), and channel surface temperature in contact with the fluid ($T_{surface}$).

6.2.1 Fluid temperature difference (ΔT_{fluid}).

In Figure 6, the variation of ΔT_{fluid} with both Re and FR is primarily governed by changes in the fluid residence time inside the channel. Increasing either Re or FR leads to higher flow velocities, which reduce the duration during which the working fluid remains in contact with the heated channel walls. As a result, the amount of thermal energy absorbed by the fluid decreases, causing a reduction in ΔT_{fluid} This behavior reflects a fundamental convective heat transfer mechanism, where the balance between flow intensity and thermal exposure time plays a dominant role in determining the fluid temperature rise, regardless of whether the operating condition is expressed in terms of Re or FR.

When ΔT_{fluid} is analyzed as a function of Re, SC generally exhibits higher temperature differences than CC. This behavior can be attributed to the reduction in hydraulic diameter caused by the presence of corrugations and winglets in the CC, which leads to higher flow velocities at a fixed Re. The resulting increase in velocity shortens the fluid residence time inside the CC, thereby limiting the amount of heat absorbed by the fluid. In contrast, ΔT_{fluid} is evaluated under FR the trend is reversed, and the CC shows higher temperature differences than the SC. Under these conditions, the flow velocity is no longer

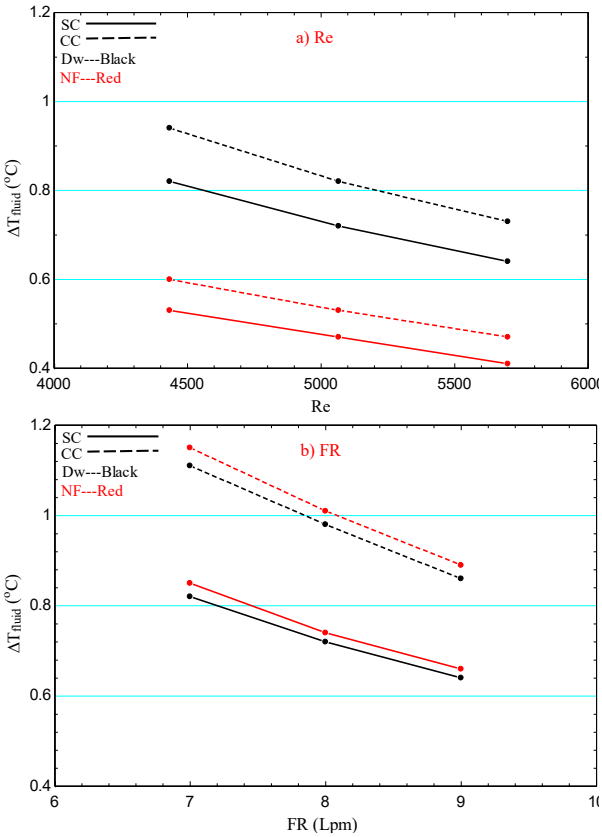

Fig 6. Effect of (a) Re and (b) FR on fluid temperature difference (ΔT_{fluid}).

constrained by Re, allowing the corrugated surfaces and winglets to enhance fluid mixing and promote stronger thermal interaction between the fluid and the channel walls.

When the analysis is based on Re, the use of NF results in lower ΔT_{fluid} values compared to DW for both channel configurations. Although NF possesses higher thermal conductivity, its increased viscosity requires higher flow velocities to maintain the same Re. This increase in velocity reduces the fluid residence time within the channel, thereby limiting the temperature rise. Conversely, when ΔT_{fluid} is evaluated under FR, the reduction associated with NF becomes less pronounced. In this case, the flow velocity is not artificially increased to satisfy Re constraint, allowing the enhanced thermal conductivity and improved mixing characteristics of NF to contribute more effectively to HT. It is therefore important to emphasize that a lower ΔT_{fluid} observed with NF usage does not indicate inferior thermal performance, but rather reflects the influence of the evaluation framework on the apparent thermal response of the system.

To further interpret the observed behavior of ΔT_{fluid} when using the nanofluid according to FR, the underlying HT mechanisms should be considered. The improvement in thermal performance observed with the TiO_2 nanofluid cannot be attributed solely to the increase in effective thermal conductivity. Several microscale transport mechanisms contribute simultaneously to the overall HT enhancement. Brownian motion of nanoparticles induces random micro-mixing within the base fluid, enhancing energy transport at the microscopic level. In addition, thermophoretic effects promote the migration of nanoparticles from hotter regions near the heated walls toward cooler core regions, contributing to continuous renewal of the thermal boundary layer. Similar enhancement mechanisms related to nanoparticle dynamics and microscale mixing have been widely reported in the literature for TiO_2-based nanofluids *(Eastman et al. 2001; Pak and Cho 1998)*.

The presence of corrugations and inclined winglets further intensifies these mechanisms by generating strong secondary flows and localized turbulence. The increased turbulence enhances nanoparticle dispersion, prevents particle agglomeration, and strengthens the interaction between nanoparticles and the surrounding fluid. As a result, the combined action of nanoparticle dynamics and geometry-induced turbulence leads to a more effective disruption of the thermal boundary layer and a noticeable enhancement in convective heat transfer.

6.2.2 Channel surface temperature ($T_{surface}$).

Figure 7 indicated that increasing either Re or FR enhances the convective heat transfer coefficient due to higher flow velocity, which promotes more effective heat extraction from the channel surface and consequently leads to a reduction in T_{surfac}.

A noticeable difference is observed between the lower and upper surfaces of CC. The lower surface generally exhibits lower temperatures, which can be attributed to the presence of winglets that locally intensify turbulence and promote strong near-wall mixing. This enhanced mixing disrupts the thermal boundary layer more effectively than the corrugated grooves on the upper surface, leading to higher local heat transfer rates and improved surface cooling at the lower wall. Consequently, the thermal performance of the winglets can be considered more effective than that of the corrugated grooves alone.

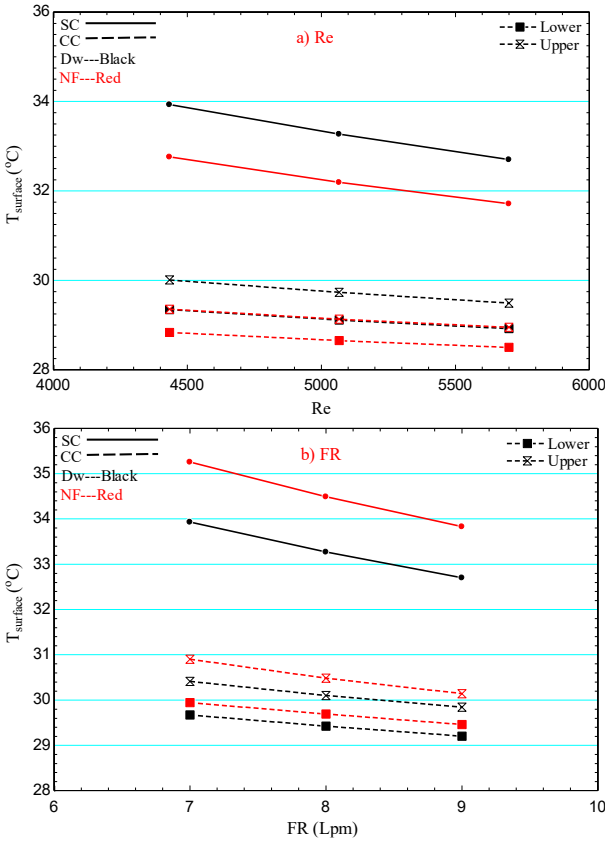

Fig 7. Effect of (a) Re and (b) FR on channel surface temperature ($T_{surface}$).

When the analysis is conducted based on Re, the use of NF leads to minimize surface temperatures. Although NF has higher thermal conductivity, its increased viscosity requires higher flow velocities to maintain the same Re, which enhances convective cooling and reduces the surface temperature. Conversely, at constant FR conditions, the higher viscosity reduces the effective flow velocity, leading to elevated wall temperatures.

It should be noted that ΔT_{fluid} and $T_{surface}$ represent local thermal indicators related to the fluid and wall temperatures, and they do not fully capture the overall thermal–hydraulic performance of the system. Therefore, relying solely on these parameters may lead to misleading conclusions when evaluating thermal performance, highlighting the necessity of using integrated performance metrics such as Nu, En, and PEC.

6.2.3 Convective heat transfer coefficient (h).

Figure 8 The variation of the convective (h) with Re and FR is primarily governed by changes in flow momentum and turbulence intensity. Increasing either Re or FR enhances convective transport, intensifies near-wall mixing, and reduces the thickness of the thermal boundary layer, which collectively leads to higher (h) values. Although Re and FR are related through their influence on flow velocity, the evaluation framework determines which physical mechanism becomes dominant.

A comparison between channel geometries indicates that the CC consistently achieves higher (h) values than SC. This enhancement is attributed to the presence of corrugations and winglets, which induce secondary flows, promote flow separation and reattachment, and generate strong localized vortices. In addition, the lower surface of CC exhibits higher (h)

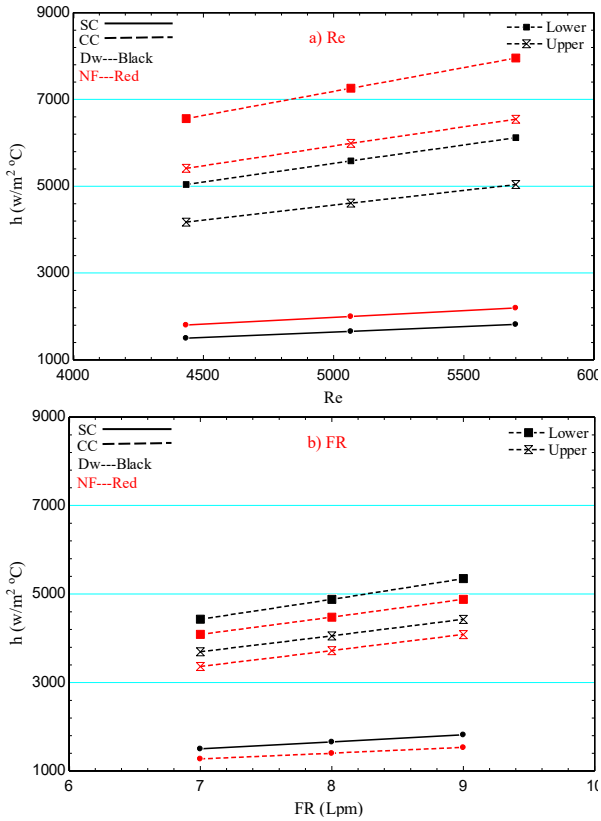

Fig 8. Effect of (a) Re and (b) FR on convective coefficient of heat transfer (h).

values than the upper surface due to the direct interaction between the flow and the winglets, which generate stronger flow disturbances compared to the grooves on the upper surface.

The influence of the working fluid depends strongly on the chosen evaluation parameter. When the analysis is conducted based on Re, the use of NF results in enhanced (h) values. Under constant Re conditions, the increased viscosity of NF necessitates higher flow velocities, causing the velocity-induced enhancement of convection to dominate and outweigh the contribution of thermal conductivity. Conversely, when (h) is evaluated at FR, the increased viscosity reduces the effective flow velocity and weakens turbulence intensity, which limits (h) despite the improved thermal conductivity of NF.

6.2.4 Pressure losses (Δp).

Figure 9 illustrates the variation of (Δp) under both Re–based and FR–based conditions for SC and CC using DW and NF. In all cases, CC exhibits higher pressure losses compared to SC due to the presence of corrugations and winglets, which intensify flow disturbances, increase wall shear stress, and enhance form drag. When the analysis is conducted based on Re, a pronounced increase in Δp is observed when using NF, particularly in the CC. This behavior is mainly attributed to the higher viscosity of NF which requires an increase in flow velocity to maintain a constant Re. The elevated velocity significantly amplifies wall friction and flow resistance, resulting in higher pressure losses.

In contrast, when Δp is evaluated under constant FR conditions, the difference between DW and NF becomes less significant. Since FR fixes the bulk flow velocity, the impact of increased viscosity is not compounded by velocity effects, leading to a more moderate rise in Δp. This comparison highlights the fundamental distinction between Re-based and FR-based representations of pressure losses, demonstrating that Δp becomes highly sensitive to velocity variations under constant Reynolds number conditions, whereas FR-based analysis provides a more direct evaluation of the hydraulic penalty associated with fluid properties and channel geometry.

Table 2 presents the normalized pumping power ratios for different reference cases over the investigated flow-rate range. As shown, the corrugated channel with winglets leads to relatively high pumping power ratios compared with the straight channel, primarily due to the strong flow disturbances induced by geometric modifications. However, it is important to note that these ratios represent relative increases with respect to a very low baseline pumping power. In absolute terms, the required pumping power remains extremely small for all investigated cases. Even at the highest operating condition (FR = 9 L/min), the maximum pumping power does not exceed approximately 0.134 W. This indicates that although the relative increase in pumping power appears significant, the actual additional energy required to circulate the fluid is negligible from a practical engineering perspective. Consequently, when combined with the consistently obtained PEC values greater than unity, the results confirm that the thermal enhancement achieved by the corrugated channel and The NF clearly outweighs the associated hydraulic penalty, making the proposed configuration suitable for practical thermal applications.

Table 2
Normalized pumping power ratios for different reference cases.

FR (LPM)	CC_{DW}/SC_{DW}	CC_{NF}/SC_{NF}	CC_{NF}/SC_{DW}
7	8.48	7.09	8.53
8	8.83	7.48	8.94
9	9.15	7.85	9.32

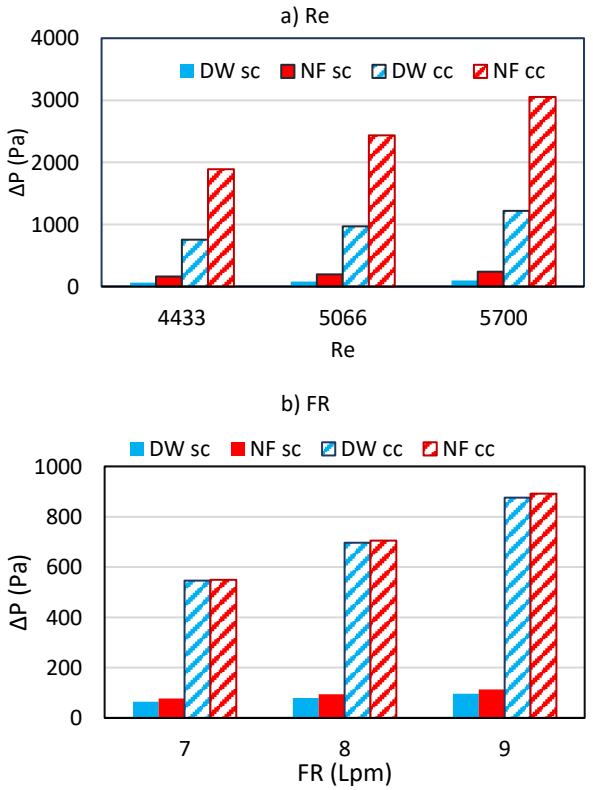

Fig 9. Variation with (a) Re and (b) FR for SC and CC using DW and NF.

6.2.5 Hydrothermal factors (Γ, En, PEC).

To better interpret the thermal–hydraulic trade-off, the performance metrics are evaluated using the following definitions:

$$\Gamma = \frac{f_{cc}}{f_{sc}} \quad (9)$$

$$En = \frac{Nu_{cc}}{Nu_{sc}} \quad (10)$$

$$PEC = \frac{E_n}{(\Gamma)^{1/3}} \quad (11)$$

Figure 10 presents a combined comparison of the relative friction factor (Γ), thermal enhancement ratio (En), and performance evaluation criterion (PEC) for DW and NF under both Re-based (a) and FR-based (b) conditions. This unified representation enables a direct assessment of the trade-off between thermal enhancement and hydraulic penalty using integrated performance indicators.

When the results are analyzed based on Re, CC exhibits a substantial increase in Γ, reflecting the higher friction losses induced by corrugations and winglets. Although this increase in flow resistance is significant, it is accompanied by a pronounced enhancement in HT, as indicated by the elevated En values. Consequently, PEC values remain consistently greater than unity for both working fluids, confirming that the thermal gains outweigh the hydraulic penalties under Re-based conditions. The slightly higher PEC values obtained with NF can be attributed to the combined effect of improved thermal conductivity and intensified flow disturbances caused by the internal structures.

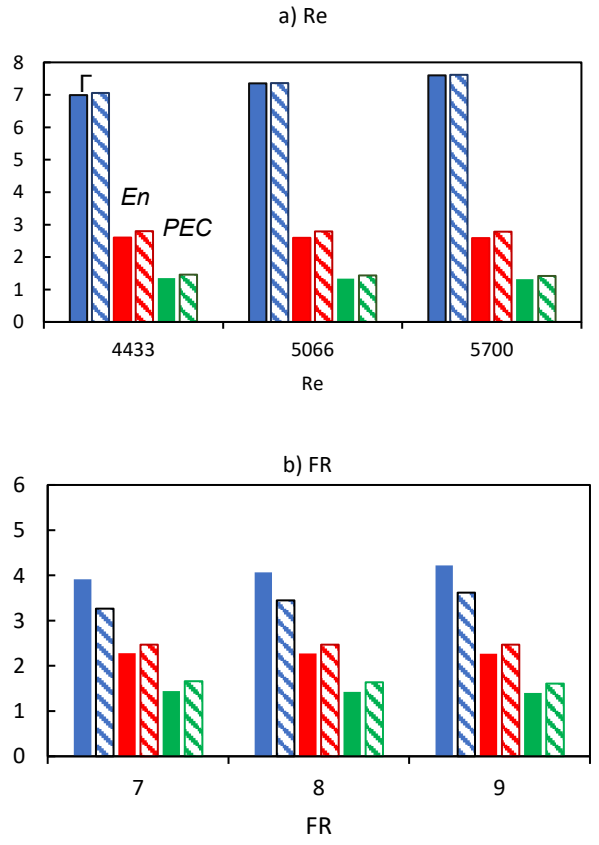

Fig 10. Comparison of Γ, En, and PEC for DW and NF at different of (a) Re and (b) FR.

In contrast, under FR-based analysis, Γ values are noticeably reduced compared to the Re-based case, as the flow velocity is fixed and not amplified by viscosity variations. While En values decrease moderately under constant FR conditions, PEC remains above unity across all tested FR. This indicates that even under more realistic operating conditions, where FR is fixed as in practical thermal systems, the combined enhancement strategy remains energetically favorable. Overall, the figure demonstrates that although Re-based analysis tends to magnify both thermal enhancement and hydraulic penalty due to velocity coupling, FR-based evaluation provides a more realistic representation of system performance. In both approaches, the PEC consistently confirms the superiority of the corrugated channel with winglets, particularly when combined with NF, validating the effectiveness of the proposed enhancement technique.

7 Conclusion

In light of the limited number of studies that have addressed the effect of FR as an alternative metric to Re in evaluating the hydrothermal performance of internal enhanced channels, this study aims to bridge an important knowledge gap. A systematic comparison was conducted between the influence of Re and FR on the thermal performance of straight and corrugated channels integrated with inclined winglets, using DW and TiO_2 nanofluid at a 1% volume concentration. The key hydrothermal parameters including (h, Δp, Γ, En, and PEC) were analyzed, along with ($T_{surface}$ and ΔT_{fluid}) of the working fluid.

The experimental results revealed that the measured thermophysical properties of the nanofluid were higher than the theoretical values, within acceptable deviations when compared to previous research. This supports the reliability of the experimental data and its applicability in numerical modeling.

The numerical simulations also showed that the presence of corrugations and winglets significantly enhanced fluid mixing and reduced stagnant increaseflow zones, which in turn minimized the boundary layer and improved (HT) efficiency, with a moderate increase in pressure losses. When comparing the Re-based and FR-based approaches, it was found that using FR offers a more realistic assessment of system behavior, especially for industrial applications operating under constant flow conditions. The hydrothermal performance indicators (e.g., PEC, En, and Γ) showed higher and more stable values when FR was used, highlighting its stronger ability to reflect the positive effect of nanofluids with high thermal conductivity. These findings underscore the importance of revisiting conventional Re only approaches and encourage considering FR as a complementary design and evaluation parameter in thermal system optimization, given its closer alignment with practical industrial operations. This confirms that performance evaluation based solely on Reynolds number may lead to misleading conclusions if velocity effects are not carefully accounted for.

The future research is recommended to explore a wider range of nanofluid concentrations and more diverse channel geometries to develop a more comprehensive understanding of physical and geometric effects. This study is distinguished by its integration of three advanced enhancement strategies (surface corrugation, inclined winglets, and nanofluid application) alongside a quantitative comparison between Re and FR systems. Together, these contributions offer a novel and practically significant step toward designing more efficient heat exchangers for industrial and renewable energy applications.

Nomenclature

h	Convective heat transfer coefficient	$W.m^{-2}.K^{-1}$
T	Temperature	°C
u	Flow velocity	$m.s^{-1}$
It	Turbulence intensity	—
Nu	Nusselt number	—
Re	Reynolds number	—
PP	pumping power	W

Greek symbols

Δp	pressure drop	Pa
λ	thermal conductivity	$W.m^{-1}.K^{-1}$
μ	Dynamic viscosity	Pa.s
ρ	Density	$kg.m^{-3}$
f	Friction factor	—
Γ	Relative friction factor	—
Φ	Volumetric concentration ratio	%

Abbreviations

BFS	Backward-Facing Step
CC	Corrugated channel
CFD	Computational fluid dynamics
DW	Distilled water
En	Thermal enhancement ratio
Exp.	Experimental
FR	Flowrate
HF	Heat flux
HT	Heat Transfer
NF	Nanofluid
Num.	Numerical
PEC	Performance evaluation criterion

References

Abed, M., Alghoul, A., Sopian, K., Mohammed, H., & Al-Shamani, N. (2015). Design characteristics of corrugated trapezoidal plate heat exchangers using nanofluids. *Chemical Engineering and Processing: Process Intensification, 87, 88–103.* https://doi.org/10.1016/j.cep.2014.11.005.

Ajeel, R., Sopian, K., & Zulkifli, R. (2021). A novel curved-corrugated channel model: thermal-hydraulic performance and design parameters with nanofluid. *International Communications in Heat and Mass Transfer,* 120, 105037; https://doi.org/10.1016/j.icheatmasstransfer.2020.105037.

Ajeel, R., Zulkifli, R., Sopian, K., Fayyadh, N., Fazlizan, A., & Ibrahim, A. (2021). Numerical investigation of binary hybrid nanofluid in new configurations for curved-corrugated channel by thermal-hydraulic performance method. *Powder Technology, 385, 144–159;* https://doi.org/10.1016/j.powtec.2021.02.055.

Ajeel, R., Sopian, K., & Rozli, Z. (2021). Thermal-hydraulic performance and design parameters in a curved-corrugated channel with l-shaped baffles and nanofluid. *Journal of Energy Storage, 34, 101996;* https://doi.org/10.1016/j.est.2020.101996.

Akçay, S. (2022). Numerical analysis of heat transfer improvement for pulsating flow in a periodic corrugated channel with discrete V-type winglets. *International Communications in Heat and Mass Transfer, 134, 105991;* https://doi.org/10.1016/j.icheatmasstransfer.2022.105991.

Akçay, S. (2023). Heat transfer analysis of pulsating nanofluid flow in a semicircular wavy channel with baffles. *Sādhanā, 48(2), 57;* https://doi.org/10.1007/s12046-023-02119-x.

Akçay, S. (2021). Investigation of thermo-hydraulic performance of nanofluids in a zigzag channel with baffles. *Adıyaman Üniversitesi Mühendislik Bilimleri Dergisi, 8(15), 525–34;* https://doi.org/10.54365/adyumbd.1000525.

Akçay, S. (2023). Numerical analysis of hydraulic and thermal performance of Al_2O_3-water nanofluid in a zigzag channel with central winglets. *Gazi University Journal of Science, 36(1), 383–397;* https://doi.org/10.35378/gujs.1012201.

Alnak, D. (2020). thermohydraulic performance study of different square baffle angles in cross-corrugated channel. *Journal of Energy Storage, 28, 101295;* https://doi.org/10.1016/j.est.2020.101295.

Bahiraei, M., & Mazaheri, N. (2020). Employing V-Shaped ribs and nanofluid as two passive methods to improve second law characteristics of flow within a square channel: a two-phase approach. *International Journal of Heat and Mass Transfer, 151, 119419;* https://doi.org/10.1016/j.ijheatmasstransfer.2020.119419.

Bazdidi, F., Karimi, M., & Jafari, M. (2011). Unsteady flow and heat transfer analysis of an impinging synthetic jet. *Heat and Mass Transfer, 47, 1363–73;* https://doi.org/10.1007/s00231-011-0801-0.

Benim, A., Himadri, C., & Ali, N. (2011). Computational analysis of turbulent forced convection in a channel with a triangular prism. *International Journal of Thermal Sciences, 50(10), 1973–83;* https://doi.org/10.1016/j.ijthermalsci.2011.05.002.

Bhowmick, D., Pitambar, R., & Sukumar, P. (2021). Implication of corrugation profile on thermo-hydraulic characteristics of Cu-water nanofluid flow through partially filled porous channel. *International Communications in Heat and Mass Transfer, 125, 105329;* https://doi.org/10.1016/j.icheatmasstransfer.2021.105329.

Çengel, Y., & Ghajar, A. (2015). Fundamentals of thermal-fluid sciences (5th ed.). *McGraw-Hill Education.*

Eastman, J., Choi, S., Li, S., Yu, W., & Thompson, L. (2001). Anomalously increased effective thermal conductivity of ethylene glycol-based nanofluids containing copper nanoparticles. *Applied Physics Letters, 78(6), 718–720;* https://doi.org/10.1063/1.1341218.

Hamad, A., & Ajeel, R. (2022). Combined effect of oblique ribs and a nanofluid on the thermal-hydraulic performance of a corrugated channel: Numerical study. *Journal of Engineering Physics and Thermophysics, 95(4), 970–978;* https://doi.org/10.1007/s10891-022-02552-5.

Hekmat, M., & Saharkhiz, S. (2022). Effect of nanofluid flows on heat transfer intensification of corrugated channels with an oscillating blade. *Chemical Engineering and Processing. 179, 109072;* https://doi.org/10.1016/j.cep.2022.109072.

Hilo, A., Antonio, A., Mohammed, T., & Mohd, H. (2020). Effect of corrugated wall combined with backward-facing step channel on fluid flow and heat transfer. *Energy, 190, 116294;* https://doi.org/10.1016/j.energy.2019.116294.

Hosseinpour, V., Karimi, M., & Rezaei, A. (2020). Developing a metamodel based upon the doe approach for investigating the overall performance of microchannel heat sinks utilizing a variety of internal fins. *International Journal of Heat and Mass Transfer, 149, 119219;* https://doi.org/10.1016/j.ijheatmasstransfer.2019.119219.

Hussein, A., Sharma, K., Bakar, R., & Kadirgama, K. (2013). The effect of nanofluid volume concentration on heat transfer and friction factor inside a horizontal tube. *Journal of Nanomaterials, 2013(1), 859563;* https://doi.org/10.1155/2013/859563.

Hussein, A., & Jawdat, A. (2021). Heat transfer enhancement using nanofluids for cooling computer device: a review. *NTU Journal of Engineering and Technology, 1(1), 25–34;* https://doi.org/10.56286/ntujet.v1i1.82.

Javadpour, S., Jahanbakhshi, E., Aghaei, O., & Ghasemi, M. (2020). Optimization of geometry and nano-fluid properties on microchannel performance using taguchi method and genetic algorithm. *International Communications in Heat and Mass Transfer, 119, 104952;* https://doi.org/10.1016/j.icheatmasstransfer.2020.104952.

Kaood, A., & Muhammed, A. (2020). Thermo-hydraulic performance of nanofluids flow in various internally corrugated tubes. *Chemical Engineering and Processing-Process Intensification, 154, 108043;* https://doi.org/10.1016/j.cep.2020.108043.

Karabulut, K. (2020). Heat transfer and pressure drop evaluation of different triangular baffle placement angles in cross-corrugated triangular channels. *Thermal Science, 24(1);* https://doi.org/10.2298/TSCI190813466K.

Koca, F. (2022). Numerical investigation of corrugated channel with backward-facing step in terms of fluid flow and heat transfer. *Journal of Engineering Thermophysics, 31(1), 187–99;* https://doi.org/10.1134/S1810232822010143.

Li, Z.-X., Sun, S.-Q., Wang, C., Liang, C.-H., Zeng, S., Zhong, T., Hu, W.-P., & Feng, C.-N. (2022). The effect of trapezoidal baffles on heat and flow characteristics of a cross-corrugated triangular duct. *Case Studies in Thermal Engineering, 33, 101903;* https://doi.org/10.1016/j.csite.2022.101903.

Murshed, S., Leong, K. & Yang, C. (2005). Enhanced thermal conductivity of TiO_2-water based nanofluids. *International Journal of Thermal Sciences, 44(4), 367–73;* https://doi.org/10.1016/j.ijthermalsci.2004.12.005.

Naderifar, A., Nazari, M., Jafari, K., & Bakhshi, M. (2022). Numerical investigation of the effect of fins on heat transfer enhancement of a laminar non-newtonian nanofluid flow through a corrugated channel. *Journal of Thermal Analysis and Calorimetry, 147(17), 9779–91;* https://doi.org/10.1007/s10973-022-11222-w.

Pak, B. C., & Cho, Y. I. (1998). Hydrodynamic and heat transfer study of dispersed fluids with submicron metallic oxide particles. *Experimental Heat Transfer an International Journal, 11(2), 151–70;* https://doi.org/10.1080/08916159808946559.

Parsaiemehr, M., Farzad, P., Omid, A., Davood, T., & Ghanbarali, S. (2018). Turbulent flow and heat transfer of water/Al_2O_3 nanofluid inside a rectangular ribbed channel. *Physica E, Low-Dimensional Systems and Nanostructures, 96, 73–84;* https://doi.org/10.1016/j.physe.2017.10.012.

Rahman, M., Shafiqul, I., & Abid, H. (2023). Numerical investigation and benchmarking of heat transfer and pressure loss characteristics with two-sided rib-roughened and two-sided heat supply in narrow rectangular channels. *Thermal Science and Engineering Progress, 41, 101812;* https://doi.org/10.1016/j.tsep.2023.101812.

Ramgadia, G., & Arun, K. (2016). Numerical study of fully developed unsteady flow and heat transfer in asymmetric wavy channels. *International Journal of Heat and Mass Transfer, 102, 98–112;* https://doi.org/10.1016/j.ijheatmasstransfer.2016.05.131.

Salami, M., Morteza, K., & Amir, F. (2019). Investigation of corrugated channel performance with different wave shapes: nanofluid as working media. *Journal of Thermal Analysis and Calorimetry, 138, 3159–74;* https://doi.org/10.1007/s10973-019-08361-y

Sedeeq, M., Ameen, S. & Bolatturk, A. (2018). Environmental impact and life cycle assessment of economically optimized thermal insulation materials for different climatic region in iraq. *International Journal of Engineering and Technology, 7(4), 163–67;* https://doi.org/10.14419/ijet.v7i4.37.24094.

Selimefendigil, F., & Hakan, F. (2020). The Potential benefits of surface corrugation and hybrid nanofluids in channel flow on the performance enhancement of a thermo-electric module in energy systems. *Energy, 213, 118520;* https://doi.org/10.1016/j.energy.2020.118520.

Shahsavar, A., Seyed, S., Ighball, B., & Hafiz, M. (2021). Numerical investigation of the effect of corrugation profile on the hydrothermal characteristics and entropy generation behavior of laminar forced convection of non-newtonian water/CMC-CuO nanofluid flow inside a wavy channel. *International Communications in Heat and Mass Transfer, 121, 105117;* https://doi.org/10.1016/j.icheatmasstransfer.2021.105117.

Shamsi, M., Omid, A., Ali, M., Davood, T., & Ramin, M. (2017). Increasing heat transfer of non-newtonian nanofluid in rectangular microchannel with triangular ribs. *Physica E, Low-Dimensional Systems and Nanostructures, 93, 167–78;* https://doi.org/10.1016/j.physe.2017.06.015.

Their, K., Abed, T., Kafel, A., & Marwa, A. (2023). thermohydraulic performance study of the effect of winglet inserts and a corrugated wall in a rectangular channel. *Case Studies in Thermal Engineering, 52, 103707;* https://doi.org/10.1016/j.csite.2023.103707.

Turgut, A., Tavman, I., Chirtoc, M., Schuchmann, H., Sauter, C., & Tavman, S. (2009). Thermal conductivity and viscosity measurements of water-based TiO_2 nanofluids. *International Journal of Thermophysics, 30(4), 1213–26;* https://doi.org/10.1007/s10765-009-0594-2.

Zhong, D., Hong, Z., & Tao, W. (2020). Investigation on the thermal properties, heat transfer and flow performance of a highly self-dispersion TiO_2 nanofluid in a multiport mini channel. *International Communications in Heat and Mass Transfer, 117, 104783;* https://doi.org/10.1016/j.icheatmasstransfer.2020.104783.